Remote sensing of atmospheric duct parameters using simulated annealing*

Zhao Xiao-Feng(赵小峰)†, Huang Si-Xun(黄思训), Xiang Jie(项 杰), and Shi Wei-Lai(施伟来)

Institute of Meteorology, PLA University of Science and Technology, Nanjing 211101, *China*

(Received 19 January 2011; revised manuscript received 19 May 2011)

Simulated annealing is one of the robust optimization schemes. Simulated annealing mimics the annealing process of the slow cooling of a heated metal to reach a stable minimum energy state. In this paper, we adopt simulated annealing to study the problem of the remote sensing of atmospheric duct parameters for two different geometries of propagation measurement. One is from a single emitter to an array of radio receivers (vertical measurements), and the other is from the radar clutter returns (horizontal measurements). Basic principles of simulated annealing and its applications to refractivity estimation are introduced. The performance of this method is validated using numerical experiments and field measurements collected at the East China Sea. The retrieved results demonstrate the feasibility of simulated annealing for near real-time atmospheric refractivity estimation. For comparison, the retrievals of the genetic algorithm are also presented. The comparisons indicate that the convergence speed of simulated annealing is faster than that of the genetic algorithm, while the anti-noise ability of the genetic algorithm is better than that of simulated annealing.

Keywords: remote sensing, refractivity estimation, electromagnetic wave propagation, simulated annealing

PACS: 92.60.Ta, 78.20.Ci, 02.30.Zz **DOI:** 10.1088/1674-1056/20/9/099201

1. Introduction

Non-standard electromagnetic propagation due to the formation of the lower atmospheric sea duct commonly occurs in maritime radar applications. Under this condition, some fundamental system parameters of seaborne radars can significantly deviate from their original values which are specified for standard refractive conditions. Knowledge of the refractivity information enables more accurate assessment of the performance of both the communications and the radar systems. Conventional methods for the refractive index measurements consist of detecting the height dependence of temperature, pressure and humidity with radiosondes, microwave refractometers, or rocketsondes have some drawbacks, such as expensive and/or difficult deployment.[1]

Richter[2] pointed out that the temporal and spatial variations of radar echoes are related to the temporal and the spatial variations of the refractivity profile, which motivates the research of the atmospheric refractivity estimation based on the radar clutter returns, i.e., refractivity from clutter (RFC). The advantage of the RFC is that it provides a synoptic characterization of the refractive index structure over the spatial extent of the radar and overcomes the necessity for additional data and/or sensing devices. In addition, the RFC has an additional advantage of being able to sense the range-varying refractivity at a temporal sampling rate that can track changes in atmospheric conditions. However, inferring the refractivity profile from the radar clutter is a complex inverse problem, because the relationship between the refractivity profile parameters and the radar clutter is clearly nonlinear and ill-posed. It is difficult to obtain analytical solutions according to current theories. The global-optimization method might be a good choice to acquire approximate solutions. Rogers *et al.*[3] inferred the evaporation duct height from radar data under the assumption of range-independent environment and sea clutter radar cross sections by using a nonlinear least square inversion procedure. Gerstoft *et al.*[4] proposed the use of the genetic algorithm (GA) to estimate the refractivity. In their work, the authors presented a method to model both the range- and the height-dependent refractivity of the environment using a total of 11 parameters,[4] and some prior constraints were imposed to increase the accuracy of the

*Project supported by the National Natural Science Foundation of China (Grant No. 40775023).

†Corresponding author. E-mail: zxf_best@126.com

© 2011 Chinese Physical Society and IOP Publishing Ltd

results over the coverage area of the radar.[5] Barrios[6] utilized the rank correlation between the observed clutter power and the density of the modeled ray paths to estimate the surface-based duct parameters. Vasudevan *et al.*[7] exploited the inherent Markovian structure of the fast Fourier transform to the parabolic equation approximation and used a particle filtering approach to retrieve the range-dependent atmospheric refractivity profile.[7] Yardim[8] adopted the Markov chain Monte Carlo (MCMC) sampling approach, the hybrid of the GA-MCMC method, and the Kalman Filters to investigate the RFC problem. Through establishing many pre-computed modeled radar returns for different environments in a database, Douvenot *et al.*[9,10] obtained real-time profiles based on the findings of the optimal environment from the database. More detailed information about the RFC technique can be found in Refs. [11]–[14].

Besides the radar clutter returns, point-to-point microwave measurements have also been proposed for the refractivity estimation. Gingras *et al.*[15] introduced basic concepts for electromagnetic matched-field processing techniques and performed a simulation of simultaneously localizing an EM emitter and estimating the atmospheric duct parameters from synthetic complex-valued field measurements. Tabrikian and Krolik[16] proposed using the point-to-point field measurements to estimate the surface-based duct parameters through the maximum a posteriori method. Gerstoft *et al.*[17] quantified the performance of matched-field processing methods for remote sensing of the refractivity structure using the signal strength measurements from a single emitter to an array of radio receivers. Valtr and Pechac[18] put forward a usage of the field measurements at a receiver site of a terrestrial point-to-point link in terms of the angle-of-arrival spectra to retrieve the vertical refractivity structure. Zhao *et al.*[19] investigated the possibilities of refractive index profile retrieval using field measurements at an array of radio receivers via the variational adjoint approach.

Simulated annealing (SA) is a technique which has attracted significant attention, as it is suited for optimization problems of large scale, especially for the case where a desired global extremum is hidden among many poorer local extrema. SA was first proposed by Kirkpatrik *et al.*[20] A description of the annealing of a molten metal motivates this algorithm. For a slowly cooling process, the inherent random fluctuation in energy allows the annealing system to escape from the local energy minimum to achieve the global minimum energy state. The SA is largely independent of the priori values and can escape from the local optimum to approach the global optimum by the uphill and the downhill moves, and it also makes few stringent assumptions regarding the functions that need to be optimized.[21]

The rest of this paper will proceed in the following manner. The atmospheric duct models are introduced in Section 2. In Section 3, a brief description of the theory of the SA is presented. In Section 4, the implementations of the SA for the atmospheric refractivity estimation are given, the vertical measurements (from a single emitter to an array of radio receivers) and the horizontal measurements (from radar clutter returns) are discussed, and the retrieved results are compared with those of the GA. Finally, the basic conclusion is summarized in Section 5.

2. Atmospheric duct models

At microwave frequencies, the atmospheric refractivity N can be expressed as

$$N = \frac{77.6}{T_{\rm a}}\left(p + \frac{4810e}{T_{\rm a}}\right), \tag{1}$$

where p is the barometric pressure in hPa, $T_{\rm a}$ is the absolute temperature in K, and e is the partial vapor pressure of water in hPa. From Eq. (1), there are two effects that can break the normal situation of an approximate linearity decrease of the refractivity in the troposphere. The first is an abrupt decrease of the water vapour pressure with height, which occurs mostly in a narrow layer over the water surface and results in the so called evaporation duct. The second is a dramatic inverse increase of the temperature with height causing the surface-based or the elevated duct in various ranges of heights. As a tool in examining refractive gradients and their effect on the propagation, a modified refractivity M is often used,

$$M = N + \frac{z}{a_{\rm e}} \times 10^6, \tag{2}$$

where z is the height above the earth's surface, and $a_{\rm e}$ is the earth's radius. The M is useful for identifying trapping layers, since the signal trapping occurs for all negative M gradients.

The three most typical ducts, the evaporation, the surface-based and the elevated ducts, are shown in Fig. 1.

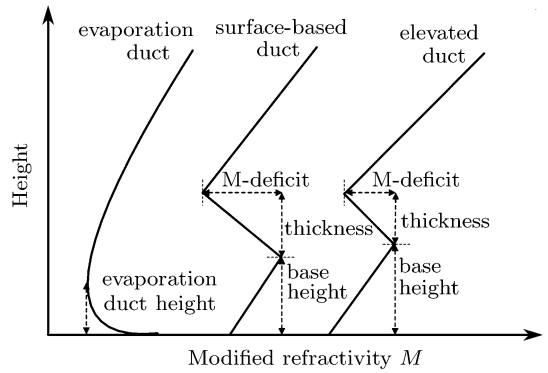


Fig. 1. Most common ducts.

The evaporation duct refractivity profiles can be constructed for thermally neutral conditions by using the log linear evaporation duct formula given by Hitney *et al.*,[22] in which the evaporation duct height (EDH) is the unique parameter to determine the duct strength. The EDH is defined by $\partial M/\partial z = 0$. The surface-based and elevated duct structures can be simply depicted by using a tri-linear refractivity profile, which is parameterized into 3 basic parameters, namely, base height, thickness, and M-deficit.[23] The base height is defined as the height from the surface of the earth to the lower boundary of the trapping layer. The thickness is defined as the distance between the lower and the upper boundaries of the trapping layer. The M-deficit is the difference between the modified refractivity values at the two boundaries of the trapping layer. The difference between the surface-based and the elevated ducts is that for the surface-based duct, the modified refractivity value at the top of the trapping layer is less than that at the surface, while for the elevated duct, the modified refractivity value at the top of the trapping layer is greater than that at the surface.

A more complicated vertical refractivity profile model consisting of 5 parameters for mixed ducts can be found in Refs. [4] and [5].

3. Inversion algorithm: simulated annealing

SA is a technique for combinatorial optimization problems, and it is robust against being trapped into the local minimum. For a global maximum case, the SA procedure begins with generating a random initial solution $\boldsymbol{x} = (x_1, x_2, \ldots, x_n)$, and the corresponding objective function value $f(\boldsymbol{x})$ is recorded. A new solution $\boldsymbol{x}'$ is chosen by varying each element of $\boldsymbol{x}$,

$$x_i' = x_i + r_i \cdot v_i, \quad i = 1, \ldots, n, \tag{3}$$

where r_i is a uniformly distributed random number from $[-1, 1]$, v_i is the i-th element of $\boldsymbol{v}$, and $\boldsymbol{v}$ is the step length for $\boldsymbol{x}$. The function value $f(\boldsymbol{x}')$ is then computed. If $f(\boldsymbol{x}')$ is greater than $f(\boldsymbol{x})$, $\boldsymbol{x}'$ is accepted, and the algorithm moves uphill. If $f(\boldsymbol{x}')$ is less than or equal to $f(\boldsymbol{x})$, the Metropolis criterion[24] is used to determine the acceptance of $\boldsymbol{x}'$. The probability

$$p_{\rm s} = \exp\left[\frac{f(\boldsymbol{x}') - f(\boldsymbol{x})}{T}\right] \tag{4}$$

is computed and compared with a uniformly distributed random number p' between 0 and 1. If $p_{\rm s}$ is greater than p', $\boldsymbol{x}'$ is accepted, and the algorithm moves downhill. Otherwise, $\boldsymbol{x}'$ is rejected. The calculation of probability $p_{\rm s}$ relies on the temperature parameter T, which plays a similar role to the temperature in the physical annealing process. To avoid getting trapped at a local optimum point, the rate of temperature reduction should be slow. The following method to reduce the temperature is usually used,

$$T_{\rm new} = \beta T_{\rm old}, \quad 0 < \beta < 1. \tag{5}$$

At the beginning of the SA, most worsening solutions may be accepted. At the end, only improving ones are likely to be allowed. This can help the procedure jump out of a local optimum. The algorithm may be terminated after the satisfaction of a certain error tolerance or after a pre-specified run time.

The performance of SA generally depends on the initial temperature T_0, the reduction rate β, and the Metropolis sampling stability. If the initial temperature is too low, the area containing the optimum might be missed; if too high, an excessively large area will be searched. Usually, T_0 could be set to be several times the maximum difference between the objective functions calculated by two possible solutions. According to Eq. (6), the objective function value f varies from (0, 1]. Thus, T_0 is set to be 1 in this paper. Considering the execution time and the annealing (not quenching) process, we set the reduction rate β to be 0.85 (suggested by Goffe *et al.*[25]). The simulated annealing code used in this paper is the SIMANN.[26]

4. Refractivity estimation

In the following, SA is first introduced to retrieve the refractivity parameters using the signal strength

measurements from a single emitter to an array of radio receivers (vertical measurements), and then it is used to investigate the refractivity estimation from the radar clutter returns (horizontal measurements). Since vertical measurement data are not available, numerical experiments are performed for the vertical measurement estimation. The horizontal measurement estimation is validated by using the field measurements collected at the East China Sea.

4.1. Vertical measurement estimation

The geometry of the observations adopted in this paper was proposed by Gingras *et al.*,[15] while the retrieval method adopted by them was the genetic algorithm.

In our simulation, an omnidirectional point source operating at 1 GHz with a height of 50 m is used. The receive antenna is a vertical array that contains 50 elements. Two strategies are considered: i) an element spacing of 1 m with the first element at 1 m above the mean sea level and a total aperture of 49 m, and ii) an element spacing of 2 m with the first element at 2 m above the mean sea level and a total aperture of 98 m. The distance between the source and the receivers is set to be 90 km. The propagation environment is a surface-based duct. The nominal values for the variable parameters are set as: M-deficit 49 M units, base height 250 m, and layer thickness 50 m. The surface value is set to be 339 M units, and the gradients at the surface and above the duct are set to be the standard modified refractivity gradient of 0.118 M units/m.

In the SA optimization, the retrieval process is to estimate the fit of the replica fields (predicted propagation measurements) with the real observation data. In our simulation, the real observation data at each receive-antenna element and the replica fields are both replaced by the modeled propagation losses $\boldsymbol{L} = (L_1, L_2, \ldots, L_n)$, which are derived from the split-step Fourier algorithm used to solve the parabolic equation.[27] The objective function could be defined as

$$f(\boldsymbol{m}) = \frac{1}{1+\phi(\boldsymbol{m})} = \max!, \tag{6}$$

$$\phi(\boldsymbol{m}) = \frac{1}{n}\sqrt{\boldsymbol{e}(\boldsymbol{m})\boldsymbol{e}^{\mathrm{T}}(\boldsymbol{m})}, \tag{7}$$

$$\boldsymbol{e}(\boldsymbol{m}) = \boldsymbol{L}_{\mathrm{obs}} - \boldsymbol{L}_{\mathrm{rep}}(\boldsymbol{m}) - (\bar{\boldsymbol{L}}_{\mathrm{obs}} - \bar{\boldsymbol{L}}_{\mathrm{rep}}), \tag{8}$$

where $\boldsymbol{m}$ is the vector of the refractivity parameter, and $\bar{\boldsymbol{L}}_{\mathrm{obs}}$ and $\bar{\boldsymbol{L}}_{\mathrm{cal}}$ are the mean values of $\boldsymbol{L}_{\mathrm{obs}}$ and $\boldsymbol{L}_{\mathrm{rep}}$, respectively. Owing to the fact that available measurements are often contaminated by noise, 10% additive white Gaussian noise is added to the synthetic field measurements. The propagation code used in this paper is the advanced propagation model (APM), which combines the capabilities of radio physical optics and the terrain parabolic equation model in a relatively fast code.[28]

To control the convergence status, the termination condition could be set as

$$1 - f(\boldsymbol{m}) < \varepsilon, \tag{9}$$

where ε is a given small positive real number used to determine the retrieval accuracy. Douvenot *et al.*[9] pointed out that operational applications of the refractivity estimation necessitate the short computation time, less than 10 min, to avoid errors due to the temporal evolution of the atmosphere. Therefore, when the computation time reaches 10 min and equation (9) is still unsatisfied, the algorithm will be terminated compulsively. Our computation equipment is a ThinkPad R400 equipped with dual CPUs (P8600, 2.40 GHz) and 2 GB EMS memory bank.

Figure 2 shows the results of the SA estimation for the case of no measurement noise. The start and the end points of each horizontal axis indicate the search bounds of the model parameters. In each experiment, the SA is run 100 times with different initial random seeds and starting values for the model parameters. Figure 2(a) shows the results with an antenna aperture size of 49 m, and figure 2(b) is for the case with an antenna aperture size of 98 m. For an error tolerance of $\varepsilon = 0.001$, the mean computation time is 242.3 s for the case shown in Fig. 2(a), and 198.4 s for the case shown in Fig. 2(b). For comparison, figure 3 gives the results of the GA. The GA search parameters are set to be population size 20, reproduction size 0.8, crossover probability 0.5, and mutation probability 0.05. For the same error tolerance, the mean computation time is 470.0 s for the case shown in Fig. 3(a), and 526.7 s for the case shown in Fig. 3(b). The probability distribution for each of the three variable M-profile parameters indicates that without the Gaussian noise, both algorithms can retrieve favourable model parameters, especially with high confidence for the base height. Moreover, SA has the advantage of fast convergence in comparison with the GA. In the estimations, the mean computation time of 49 m aperture size is longer than that of 98 m aperture size when using SA, while an opposite phenomenon occurs when using the GA.

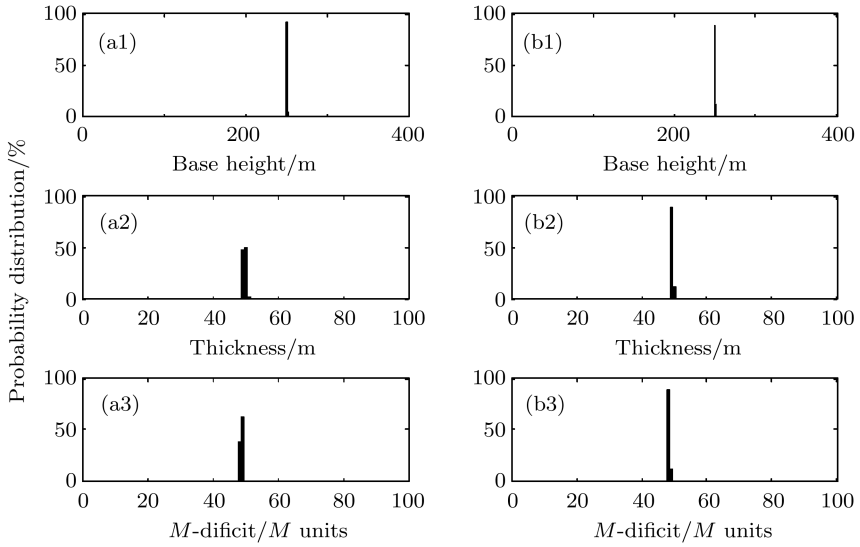


Fig. 2. Retrievals without Gaussian noise in measurement data by SA: (a1)–(a3) inversions of 49 m aperture size, (b1)–(b3) inversions of 98 m aperture size.

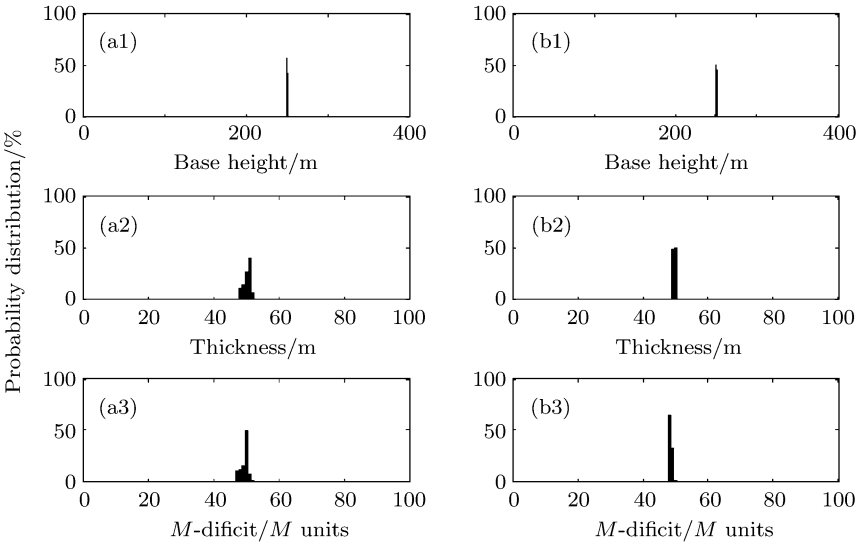


Fig. 3. Retrievals without Gaussian noise in measurement data by the GA: (a1)–(a3) inversions of 49 m aperture size, (b1)–(b3) inversions of 98 m aperture size.

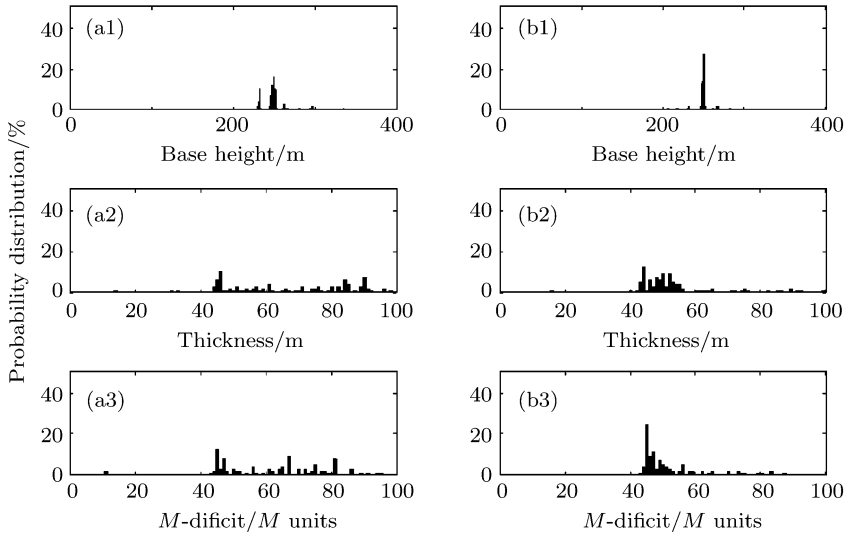


Fig. 4. Retrievals with 10% Gaussian noise in measurement data by SA: (a1)–(a3) inversions of 49 m aperture size, (b1)–(b3) inversions of 98 m aperture size.

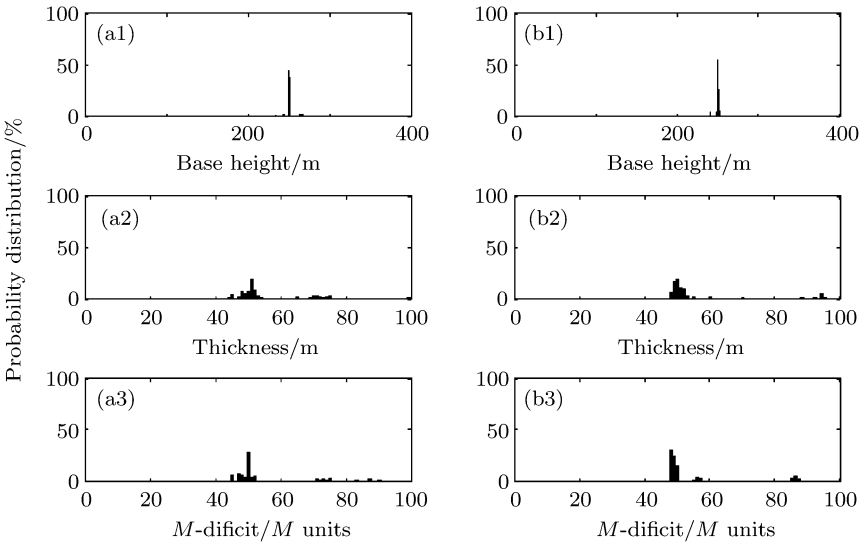


Fig. 5. Retrievals with 10% Gaussian noise in measurement data by the GA: (a1)–(a3) inversions of 49 m aperture size, (b1)–(b3) inversions of 98 m aperture size.

Figure 4 shows the results of the SA estimation for the case with 10% Gaussian noise added to the measurement data. In this case, owing to the uncertainty of the noise, the termination condition is only controlled by the computation time of 10 min. Figure 5 shows the results of the GA. The probability distributions of the retrieved parameters indicate that the Gaussian noise makes the inversions become ill-posed. Comparing Fig. 4 with Fig. 5, the retrieved results of the GA are slight better than those of SA, which means the anti-noise ability of the GA is superior for the refractivity estimation. In both algorithms, the inversion of 98 m aperture size is better than that of 49 m aperture size, even though both antenna arrays have the same number of elements and the smaller array samples a high-amplitude region of the signal field more densely. This phenomenon demonstrates that extensively special sampling could obtain more signal field characteristics and is better than centralized sampling. In Figs. 4 and 5, except for the base height, the other two parameters are not concentrated around the actual values. However, an approximate value might be judged based on their distributions.

4.2. Horizontal measurement estimation

In horizontal measurement estimations, the field measurement data collected at the East China Sea are used to validate the remote sensing of refractivity from the radar clutter returns using SA. Firstly, a forward simulation of the observed radar clutter power should be performed. By using the classical radar equation, the observed radar clutter power could be calculated as[4]

$$P_{\rm obs}(r) = -2L(r, \boldsymbol{m}) + 10\lg(r) + \sigma^0(r) + C, \quad (10)$$

where L is the propagation loss, r is the horizontal distance, σ^0 is the radar cross section (RCS) of the sea surface at range r, and C is a constant taking into account the radar parameters including wavelength, transmitter power, antenna gain, etc. From Eq. (10), it can be seen that if we want to obtain an accurate radar sea clutter power $P_{\rm obs}$, L and σ^0 must be calculated accurately. Here, L is generated from the parabolic equation, and σ^0 is calculated by using the adjusted Barton model.[13] Gerstoft *et al.*[4] pointed out that in the refractivity estimations, the horizontal variations in the RCS computations are not critical.[4] Thus, in our calculations, the RCS is assumed to be range-independent. Using the radar clutter power, equation (8) of the objective function should be modified to

$$e(\boldsymbol{m}) = \boldsymbol{P}_{\rm obs} - \boldsymbol{P}_{\rm rep}(\boldsymbol{m}) - (\bar{\boldsymbol{P}}_{\rm obs} - \bar{\boldsymbol{P}}_{\rm rep}), \quad (11)$$

where $\bar{\boldsymbol{P}}_{\rm obs}$ and $\bar{\boldsymbol{P}}_{\rm cal}$ are the mean values of $\boldsymbol{P}_{\rm obs}$ and $\boldsymbol{P}_{\rm rep}$, respectively.

The experiment conducted at the East China Sea is for the evaporation duct detection case. Modified refractivity M for an evaporation duct can be determined at any height z by using the logarithmic linear formula given by Hitney *et al*,[22]

$$M(z) = M_0 + 0.125z - 0.125d\ln[(z + z_0)/z_0], \quad (12)$$

where M_0 is the modified refractivity at the sea surface, d is the evaporation duct height (EDH), and z_0 is the Jeske's roughness length of 1.5×10^{-4} m. The

EDH generally varies between 0 m and 40 m. Therefore, the search bounds of the EDH are set to be from 0 m to 40 m.

The parameters of the radar system used in the experiment are shown in Table 1. Detailed descriptions of the experiment can be found in Refs. [13] and [29].

Table 1. Parameters of the radar system.

Parameter	Value
Frequency	10 GHz
Beam width	0.7°
Antenna height	10 m
Polarization	HH[a)]
Range bin width	500 m

[a)] HH stands for horizontal-to-horizontal.

For the evaporation duct model, only one parameter, i.e., EDH, needs to be estimated. From the root mean square error analysis by Wang *et al.*,[13] the observed EDH is 13 m (see Fig. 7). In consideration of the search bounds of the EDH, numerous iterations become meaningless and unnecessary. In this section, the termination condition is set to be 1 min. Figure 6 shows the probability distribution of the retrievals, and Table 2 shows the statistics of the results. It can be seen that for a given observation, SA has better convergence than the GA. However, the final aim of the refractivity estimation is not to give the exact refractivity profile, but to propose a generic structure that is able to render an approximation of the real atmospheric conditions.[9] From this point of view, both retrievals are acceptable.

Table 2. Statistics of the retrieved results.

Methods	Min/m	Max/m	Mean/m
SA	12.33	13.18	12.88
GA	12.12	13.76	12.82

Figure 7 shows an example of the retrievals. Figure 7(a) gives the observed refractivity profile (solid line) and the mean value of the retrieved profiles by the SA (dashed line). Figure 7(b) shows the observed clutter power (solid line), the replica clutter power computed by the retrieved profile (dashed line), and the replica clutter power computed by the observed profile (dotted line). From Fig. 7(b), it can be seen that not only the replica power computed by the retrieved profile but also the replica power computed by the observed profile does not match well with the observed data. This phenomenon might be attributed to the following reasons: 1) errors stem from the forward model and the measurement noise, 2) the chosen model for the refractivity is too simple, 3) the range-independent assumption of the environment is not valid, 4) the difficulty accurately computing the sea-clutter RCS. However, through a simple least square objective function, the best matching replica power can be judged by examining the matching degree of the peaks in the replica field.

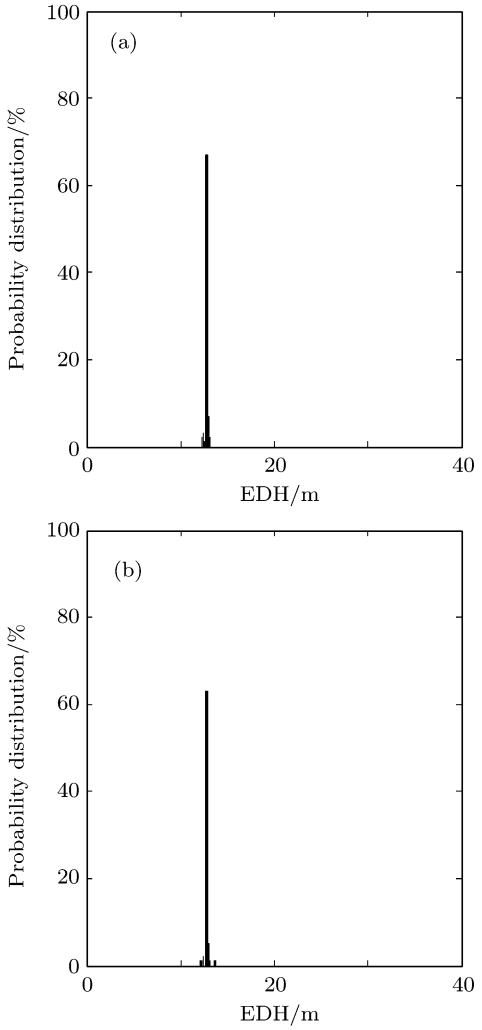


Fig. 6. Retrieved evaporation duct heights from radar sea clutter using (a) simulated annealing and (b) genetic algorithm.

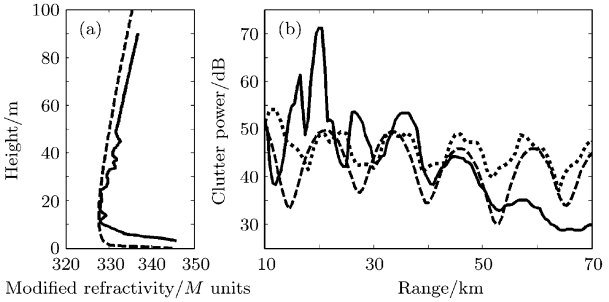


Fig. 7. (a) Modified refractivity profiles and (b) corresponding radar clutter powers.

It should be pointed out that the range bin width is determined by the pulse width of the radar, and the measured clutter is only one value in each range. Hence we typically approximate the signal that is scattered in a given range from the parabolic equation field at 1 m above the surface. On the other hand, using the parabolic equation to simulate the field measurements in the troposphere cannot obtain correct results for very short range. Therefore, the first 10 km of clutter power data deviating from the source are ignored in the inversion process.

5. Conclusion

In this paper, the problem of the remote sensing of the atmospheric refractivity parameters using SA is addressed. The inversion problem is investigated for two different geometries of propagation field measurements. The parabolic equation solved by the split-step Fourier algorithm is used as the forward propagation model. In the estimations, the retrieved results are compared with those of the GA. Two scales of the receiver array are studied in the vertical measurement inversions, and the results demonstrate that the inversions are satisfied under the no noise assumption, and SA presents a rather faster convergence. For the 10% white Gaussian noise case, the inversions are corrupted except for the base height. In the horizontal measurement inversions, an evaporation duct profile and the corresponding radar sea clutter collected at the East China Sea are analysed. Though the replica field did not match well with the observed data, from a simple least square objective function, the best matching signal power could be approached by examining the degree of compliance of the locations of the maximum and the minimum in the replica field. The simulations and the real data results demonstrate the applicability of SA for refractivity estimation. The validations of SA in practical applications should be tested further by more real data experiments.

Acknowledgment

The authors would like to thank Dr. Wang for his suggestion to obtain the real data collected at the East China Sea from Ref. [13].

References

[1] Halvey R A 1983 *Proc. IEEE* Part F **130** 643
[2] Richter J H 1969 *Radio Sci.* **4** 1261
[3] Rogers L T, Hattan C P and Stapleton J K 2000 *Radio Sci.* **35** 955
[4] Gerstoft P, Rogers L T, Krolik J L and Hodgkiss W S 2003 *Radio Sci.* **38** 8053
[5] Gerstoft P, Rogers L T, Hodgkiss W S and Wagner L J 2003 *IEEE J. Oceanic Eng.* **28** 513
[6] Barrios A E 2004 *Radio Sci.* **39** RS6013
[7] Vasudevan S, Anderson R H, Kraut S, Gerstoft P, Rogers L T and Krolik J 2007 *Radio Sci.* **42** RS2014
[8] Yardim C 2007 *Statistical Estimation and Tracking of Refractivity from Radar Clutter* (Ph.D. Dissertation) (San Diego: University of California San Diego)
[9] Douvenot R, Fabbro V, Gerstoft P, Bourlier C and Saillard J 2008 *Radio Sci.* **43** RS6005
[10] Douvenot R, Fabbro V, Gerstoft P, Bourlier C and Saillard J 2010 *Radio Sci.* **45** RS1007
[11] Huang S X, Zhao X F and Sheng Z 2009 *Chin. Phys.* B **18** 5084
[12] Sheng Z, Huang S X and Zhao X F 2009 *Acta Phys. Sin.* **58** 6627 (in Chinese)
[13] Wang B, Wu Z S, Zhao Z W and Wang H G 2009 *Prog. Electromagn. Res.* M **9** 79
[14] Zhao X F, Huang S X and Sheng Z 2010 *Chin. Phys.* B **19** 049201
[15] Gingras D F, Gerstoft P and Gerr N L 1997 *IEEE Trans. Antennas Propagat.* **45** 1536
[16] Tabrikian J and Krolik J L 1999 *IEEE Trans. Antennas Propag.* **47** 1727
[17] Gerstoft P, Gingras D F, Rogers L T and Hodgkiss W S 2000 *IEEE Trans. Antennas Propagat.* **48** 345
[18] Valtr P and Pechac P 2005 *XXVIIIth General Assembly of International Union of Radio Science*, October 23–29, 2005, New Delhi, India
[19] Zhao X F, Huang S X and Du H D 2011 *Radio Sci.* **46** RS1006
[20] Kirkpatrick S, Gelatt C D and Vecchi M P 1983 *Science* **220** 671
[21] Lam J 1988 *An Efficient Simulated Annealing Schedule* (Ph.D. Dissertation) (New Haven: Yale University)
[22] Hitney H V and Vieth R 1990 *IEEE Trans. Antennas Propag.* **38** 794
[23] Rogers L T 1997 *Radio Sci.* **32** 79
[24] Metropolis N, Rosenbluth A W, Rosenbluth M N, Teller A H and Teller E 1953 *J. Chem. Phys.* **21** 1087
[25] Goffe W L, Ferrier G D and Rogers J 1994 *J. Econometrics* **60** 65
[26] http://emlab.berkeley.edu/Software/abstracts/goffe895.html
[27] Kuttler J R and Dockery G D 1991 *Radio Sci.* **26** 381
[28] Barrios A E and Patterson W L 2002 *Advanced Propagation Model (APM) Ver. 1.3.1 Computer Software Configuration Item (CSCI) Documents* Technical Document 3145, San Diego, California
[29] Wang B, Wu Z S, Zhao Z W and Wang H G 2009 *Chin. J. Radio Sci.* **24** 598 (in Chinese)